

Chapter 4

System - HONO₂

One of the key steps in the investigation of ultrafast photoinduced dynamics of molecules is the choice of a proper model for the description of the system. This step is not trivial, especially in systems with many degrees of freedom. A good model should be specific enough to adequately represent the relevant physical effects, and yet simple enough to be computationally feasible. In this chapter a novel model for studying the vibrational dynamics of a nitric acid (HONO₂) molecule in the gas phase (Figure 4.1) induced by ultrashort laser pulses shall be presented.

The dynamics shall be investigated in three dimensions, corresponding to three vibrational degrees of freedom, represented by the natural molecular coordinates, consisting of two bond lengths (the ON single bond and the OH bond), and the bending angle between them. Since no assumptions shall be introduced for the amplitudes of vibrations, the model is suitable for treatment of dissociation, large amplitude bending vibration, and can naturally accommodate different molecular conformations [110]. The model is by no means restricted to a particular system, and can in fact be applied to any planar nonrotating asymmetric triatomic molecule.

For the proposed model, the vibrational Hamilton operator shall be derived, which is free from singular terms (see, e.g. references [111–115]) in the vicinity of linear configuration (bending angle $\alpha \approx \pi$), and smoothly transforms into the

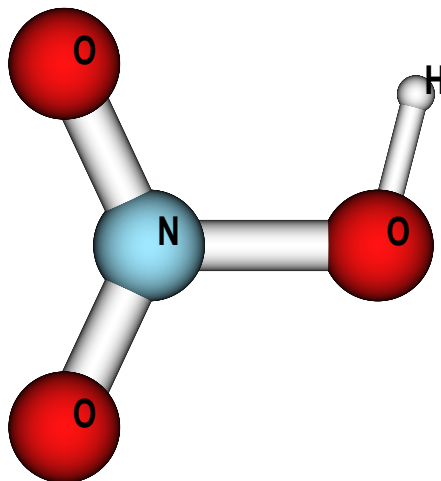


Figure 4.1: The nitric acid molecule.

Hamilton operator of a linear molecule when $\alpha = \pi$. This enables the investigation of large amplitude bending vibrations, even the ones that pass through the linear molecular configuration.

To illustrate the potential of the model, two exemplary applications shall be considered: the investigation of the restricted IVR in the OH bond, involving free evolution and preparation of the zeroth-order OH states, and highly selective ON bond breaking of the HONO₂ molecule. The task of finding the optimal laser fields for both problems was performed by Dr. G.K. Paramonov. The results of this chapter are published in [116]. For a more systematic study of the restricted IVR and bond-selective dissociation in HONO₂ the reader is referred to Ref. [117].

4.1 Model, equation of motion, and technique

4.1.1 Derivation of the molecular Hamiltonian

Let us consider the nonrotating HONO₂ molecule lying in the (x, y) plane. Translational motion shall not be taken into account. The NO₂ fragment is treated at its equilibrium configuration, and represented by a single particle at its center of mass, which reduces the model to that of a nonrotating asymmetric triatomic ABC molecule. The number of system degrees of freedom in this case reduces to three, which shall be represented by the natural molecular coordinates, namely the lengths of the ON single (r_1) and OH (r_2) bonds, and the bending angle (α) between them (see Figure 4.2). The molecular Hamiltonian operator then reads:

$$\hat{H}_{\text{mol}}(r_1, r_2, \alpha) = \hat{T} + \hat{V}(r_1, r_2, \alpha). \quad (4.1)$$

The potential energy term $\hat{V}(r_1, r_2, \alpha)$ in equation (4.1) has been defined *ab initio* [110]. Below the derivation of the kinetic energy operator \hat{T} is outlined in detail.

The starting point for the derivation is the kinetic energy operator written in Cartesian coordinates in a laboratory reference frame:

$$\hat{T} = -\frac{\hbar^2}{2m_1} \left(\frac{\partial^2}{\partial x_1^2} + \frac{\partial^2}{\partial y_1^2} \right) - \frac{\hbar^2}{2m_2} \left(\frac{\partial^2}{\partial x_2^2} + \frac{\partial^2}{\partial y_2^2} \right) - \frac{\hbar^2}{2m_3} \left(\frac{\partial^2}{\partial x_3^2} + \frac{\partial^2}{\partial y_3^2} \right), \quad (4.2)$$

where $x_i, y_i; i = 1, 2, 3$ are Cartesian coordinates of the center of mass of the NO₂ fragment, central O atom and the H atom respectively, $m_1 = m(\text{NO}_2), m_2 = m(\text{O}), m_3 = m(\text{H})$.

First, it is appropriate to change to the coordinate system consisting of the center of mass positions and projections of the bond lengths on Cartesian axes. In matrix

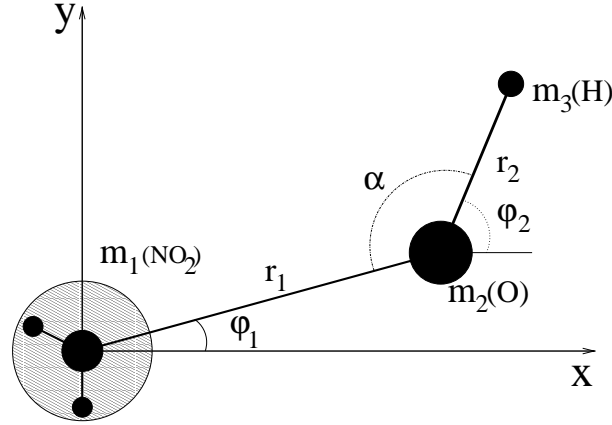


Figure 4.2: The HONO₂ molecule and the relevant coordinates. The NO₂ fragment (encircled and scaled down) is treated as one particle.

form,

$$\begin{pmatrix} x_0 \\ y_0 \\ l_{x_1} \\ l_{y_1} \\ l_{x_2} \\ l_{y_2} \end{pmatrix} = \begin{pmatrix} m_1/M & 0 & m_2/M & 0 & m_3/M & 0 \\ 0 & m_1/M & 0 & m_2/M & 0 & m_3/M \\ -1 & 0 & 1 & 0 & 0 & 0 \\ 0 & -1 & 0 & 1 & 0 & 0 \\ 0 & 0 & -1 & 0 & 1 & 0 \\ 0 & 0 & 0 & -1 & 0 & 1 \end{pmatrix} \begin{pmatrix} x_1 \\ y_1 \\ x_2 \\ y_2 \\ x_3 \\ y_3 \end{pmatrix}. \quad (4.3)$$

Here x_0, y_0 are the Cartesian coordinates of the center of mass, $M = m_1 + m_2 + m_3$ is the total mass, $l_{x_i}, l_{y_i}; i = 1, 2$ are the projections of the ON and OH bonds, respectively, on the x and y axes. In compact form equation (4.3) can be rewritten as

$$X_{new} = AX_{old}. \quad (4.4)$$

The corresponding conjugate momenta

$$\hat{p}_j = -i \frac{\partial}{\partial x_j} \quad (4.5)$$

transform according to the following equation [118])

$$\mathbf{P}_{\text{old}} = \mathbf{A}^T \mathbf{P}_{\text{new}}, \quad (4.6)$$

where \mathbf{A} is the transformation matrix from equation (4.3). Solution of equation (4.6) gives us the old momenta in Cartesian coordinates as functions of new ones, and substituting these solutions into equation (4.2) gives the following expression for the kinetic energy operator:

$$\begin{aligned} \hat{\mathbf{T}} = & -\frac{\hbar^2}{2\mu_1} \frac{\partial^2}{\partial l_{x_1}^2} - \frac{\hbar^2}{2\mu_1} \frac{\partial^2}{\partial l_{y_1}^2} - \frac{\hbar^2}{2\mu_2} \frac{\partial^2}{\partial l_{x_2}^2} - \frac{\hbar^2}{2\mu_2} \frac{\partial^2}{\partial l_{y_2}^2} \\ & + \frac{\hbar^2}{m_2} \frac{\partial^2}{\partial l_{x_1} \partial l_{x_2}} + \frac{\hbar^2}{m_2} \frac{\partial^2}{\partial l_{y_1} \partial l_{y_2}} - \frac{\hbar^2}{2M} \frac{\partial^2}{\partial x_0^2} - \frac{\hbar^2}{2M} \frac{\partial^2}{\partial y_0^2}. \end{aligned} \quad (4.7)$$

Here the reduced masses $\mu_1 = m_1 m_2 / (m_1 + m_2)$ and $\mu_2 = m_2 m_3 / (m_2 + m_3)$ of the ON and OH bonds respectively are introduced. The last two terms in (4.7) correspond to the translational motion of the molecule, which can be separated from the Schrödinger equation and disregarded.

Now from the center-of-mass and bond length coordinates we change to a polar coordinate system of bond lengths and angles $(r_i, \phi_i; i = 1, 2)$ (see figure 4.2). These coordinate transformation reads as follows:

$$\begin{aligned} l_{x_1} &= r_1 \cos \phi_1, \\ l_{y_1} &= r_1 \sin \phi_1, \\ l_{x_2} &= r_2 \cos \phi_2, \\ l_{y_2} &= r_2 \sin \phi_2. \end{aligned} \quad (4.8)$$

We proceed by expressing the momenta of equation (4.7) in terms of the momenta conjugate to (r_i, ϕ_i) coordinates by applying the chain rule of differentiation. The calculation is straightforward, albeit tedious, and was performed using the Mathe-

matica 3.0 symbolic mathematics package. We obtain:

$$\begin{aligned}
\hat{T} = & -\frac{\hbar^2}{2\mu_1} \frac{\partial^2}{\partial r_1^2} - \frac{\hbar^2}{2\mu_2} \frac{\partial^2}{\partial r_2^2} - \frac{\hbar^2}{2\mu_1 r_1^2} \frac{\partial^2}{\partial \phi_1^2} - \frac{\hbar^2}{2\mu_2 r_2^2} \frac{\partial^2}{\partial \phi_2^2} \\
& - \frac{\hbar^2}{2\mu_1 r_1} \frac{\partial}{\partial r_1} - \frac{\hbar^2}{2\mu_2 r_2} \frac{\partial}{\partial r_2} \\
& + \frac{\hbar^2 \cos(\phi_1 - \phi_2)}{m_2} \frac{\partial^2}{\partial r_1 \partial r_2} + \frac{\hbar^2 \cos(\phi_1 - \phi_2)}{m_2 r_1 r_2} \frac{\partial^2}{\partial \phi_1 \partial \phi_2} \\
& + \frac{\hbar^2 \sin(\phi_1 - \phi_2)}{m_2 r_2} \frac{\partial^2}{\partial r_1 \partial \phi_2} - \frac{\hbar^2 \sin(\phi_1 - \phi_2)}{m_2 r_1} \frac{\partial^2}{\partial r_2 \partial \phi_1}.
\end{aligned} \tag{4.9}$$

The transformation to polar coordinates gives the following expression for the volume element : $d\tau = r_1 r_2 dr_1 dr_2 d\phi_1 d\phi_2$, which is dependent on r_i . However, to calculate the observables we are interested in evaluating integrals involving quadratic combinations of the wave functions. The following similarity transformation

$$\Phi(r_1, r_2, \phi_1, \phi_2) = \Psi(r_1, r_2, \phi_1, \phi_2) \sqrt{r_1 r_2}, \tag{4.10}$$

allows to avoid the $r_1 r_2$ product in the volume element. Here Ψ is the original wave function, and Φ is the wave function that shall be used in all subsequent calculations.

The kinetic energy operator (4.9) then becomes

$$\begin{aligned}
\hat{T} = & -\frac{\hbar^2}{2\mu_1} \frac{\partial^2}{\partial r_1^2} - \frac{\hbar^2}{2\mu_2} \frac{\partial^2}{\partial r_2^2} - \frac{\hbar^2}{2\mu_1 r_1^2} \frac{\partial^2}{\partial \phi_1^2} - \frac{\hbar^2}{2\mu_2 r_2^2} \frac{\partial^2}{\partial \phi_2^2} \\
& - \frac{\hbar^2 \cos(\phi_1 - \phi_2)}{2m_2 r_2} \frac{\partial}{\partial r_1} - \frac{\hbar^2 \cos(\phi_1 - \phi_2)}{2m_2 r_1} \frac{\partial}{\partial r_2} \\
& + \frac{\hbar^2 \sin(\phi_1 - \phi_2)}{2m_2 r_1 r_2} \frac{\partial}{\partial \phi_1} - \frac{\hbar^2 \cos(\phi_1 - \phi_2)}{2m_2 r_1 r_2} \frac{\partial}{\partial \phi_2} \\
& + \frac{\hbar^2 \cos(\phi_1 - \phi_2)}{m_2} \frac{\partial^2}{\partial r_1 \partial r_2} + \frac{\hbar^2 \cos(\phi_1 - \phi_2)}{m_2 r_1 r_2} \frac{\partial^2}{\partial \phi_1 \partial \phi_2} \\
& + \frac{\hbar^2 \sin(\phi_1 - \phi_2)}{m_2 r_2} \frac{\partial^2}{\partial r_1 \partial \phi_2} - \frac{\hbar^2 \sin(\phi_1 - \phi_2)}{m_2 r_1} \frac{\partial^2}{\partial r_2 \partial \phi_1} \\
& + \frac{\hbar^2 \cos(\phi_1 - \phi_2)}{4m_2 r_1 r_2} - \frac{\hbar^2}{8\mu_1 r_1^2} - \frac{\hbar^2}{8\mu_2 r_2^2}.
\end{aligned} \tag{4.11}$$

The last three ‘potential-like’ terms in this expression are a direct consequence of the transformation (4.10).

We consider our molecule to be non-rotating ($J = 0$). The total angular momentum has only the L_z component, since we assume the molecule to be constrained to

(x, y) plane. The angular momentum conservation law therefore requires $L_z = 0$. Expanding the latter equation in Cartesian coordinates gives:

$$\hat{L}_z = i \sum_{i=1}^3 \left(y_i \frac{\partial}{\partial x_i} - x_i \frac{\partial}{\partial y_i} \right) = 0. \quad (4.12)$$

After changing to polar coordinates, we obtain

$$\hat{L}_z = -\frac{\partial}{\partial \phi_1} - \frac{\partial}{\partial \phi_2} = 0. \quad (4.13)$$

It is reasonable to redefine the angular variables in a way which makes the kinetic energy operator invariant with respect to the laboratory frame of reference. This may be achieved by the following transformation of angular coordinates:

$$\begin{aligned} \phi_+ &= \phi_2 + \phi_1, \\ \phi_- &= \phi_2 - \phi_1. \end{aligned} \quad (4.14)$$

The momenta conjugate to ϕ_+ vanish due to the momentum conservation constraint, and the kinetic energy operator is dependent only on the angle ϕ_- between ON and OH bonds.

After substituting (4.13) and (4.14) in (4.11), and redefining $\phi_- = \pi - \alpha$, we finally obtain:

$$\begin{aligned} \hat{T} = & -\frac{\hbar^2}{2\mu_1} \frac{\partial^2}{\partial r_1^2} - \frac{\hbar^2}{2\mu_2} \frac{\partial^2}{\partial r_2^2} - \frac{\hbar^2 \cos \alpha}{m_2} \frac{\partial^2}{\partial r_1 \partial r_2} \\ & + \frac{\hbar^2 \cos \alpha}{2m_2} \left(\frac{1}{r_2} \frac{\partial}{\partial r_1} + \frac{1}{r_1} \frac{\partial}{\partial r_2} \right) \\ & - \left(\frac{\hbar^2}{2\mu_1 r_1^2} + \frac{\hbar^2}{2\mu_2 r_2^2} - \frac{\hbar^2 \cos \alpha}{m_2 r_1 r_2} \right) \frac{\partial^2}{\partial \alpha^2} - \frac{\hbar^2 \sin \alpha}{2m_2 r_1 r_2} \frac{\partial}{\partial \alpha} \\ & + \frac{\hbar^2 \sin \alpha}{m_2} \left(\frac{1}{r_2} \frac{\partial}{\partial r_1} + \frac{1}{r_1} \frac{\partial}{\partial r_2} \right) \frac{\partial}{\partial \alpha} \\ & - \frac{\hbar^2 \cos \alpha}{4m_2 r_1 r_2} - \frac{\hbar^2}{8\mu_1 r_1^2} - \frac{\hbar^2}{8\mu_2 r_2^2}. \end{aligned} \quad (4.15)$$

For the integration of the wave functions, the volume element is $d\tau = dr_1 dr_2 d\alpha$.

The kinetic energy operator (4.15) is very similar to those already known (see, for example, equation (78) in Ref. [111]). The only difference, which is nevertheless

important, is the absence of two singular ‘‘potential-type’’ terms in the equation (4.15),

$$\frac{\hbar^2 \cos \alpha}{4m_2 r_1 r_2 \sin^2 \alpha} + \frac{\hbar^2}{8 \sin^2 \alpha} \left(\frac{1}{\mu_1 r_1^2} + \frac{1}{\mu_2 r_2^2} \right), \quad (4.16)$$

which do appear in equation (78) in Ref. [111]. These terms are not significant in the vicinity of the equilibrium configuration, but they prohibit the investigation of dynamics in the vicinity of the bending angle $\alpha = \pi$. In contrast, equation (4.15) allows the smooth transition through the ‘linear’ configuration, which enables us to study the processes with the linear configuration as transition state, such as the selective preparation of conformers in HONO₂ [110]. For a discussion on the origin of the singular terms in the Hamiltonian, see Appendix C.

4.1.2 Basis set and interaction with the laser field

For the problem of monitoring the IVR in HONO₂ molecule the direct product of one-dimensional zeroth-order states of individual vibrational modes is used as the basis set. To calculate these zeroth-order states, the following zeroth-order Hamiltonians are formulated by fixing all but one of the degrees of freedom at their equilibrium values, analogously to [111], as suggested by G.K. Paramonov [110]:

$$\hat{H}_{r_1}^0(r_1) = \hat{H}_{\text{mol}}(r_1, r_2 = r_2^{eq}, \alpha = \alpha^{eq}), \quad (4.17)$$

$$\hat{H}_{r_2}^0(r_2) = \hat{H}_{\text{mol}}(r_1 = r_1^{eq}, r_2, \alpha = \alpha^{eq}), \quad (4.18)$$

$$\hat{H}_{\alpha}^0(\alpha) = \hat{H}_{\text{mol}}(r_1 = r_1^{eq}, r_2 = r_2^{eq}, \alpha). \quad (4.19)$$

Then the corresponding time-independent Schrödinger equations

$$\hat{H}_{r_1}^0 |\psi_n^0\rangle = E_n^0 |\psi_n^0\rangle, \quad (4.20)$$

$$\hat{H}_{r_2}^0 |\phi_m^0\rangle = E_m^0 |\phi_m^0\rangle, \quad (4.21)$$

$$\hat{H}_{\alpha}^0 |\chi_k^0\rangle = E_k^0 |\chi_k^0\rangle. \quad (4.22)$$

give the zeroth-order vibrational eigenenergies and eigenstates for each of the degrees of freedom.

The equations (4.20) and (4.21) were solved by the Fourier grid Hamiltonian (FGH) method [72], and for equation (4.22) a DVR method was used, with extensions necessary to allow treatment of first order derivatives in the zeroth-order Hamiltonian \hat{H}_α^0 . The calculated frequency of the transition to the first excited zeroth-order bending state, 1306.8 cm⁻¹ is in good agreement with the spectroscopic data, which gives $\nu_4 = 1303$ cm⁻¹ [119]. The first ten zeroth-order bending

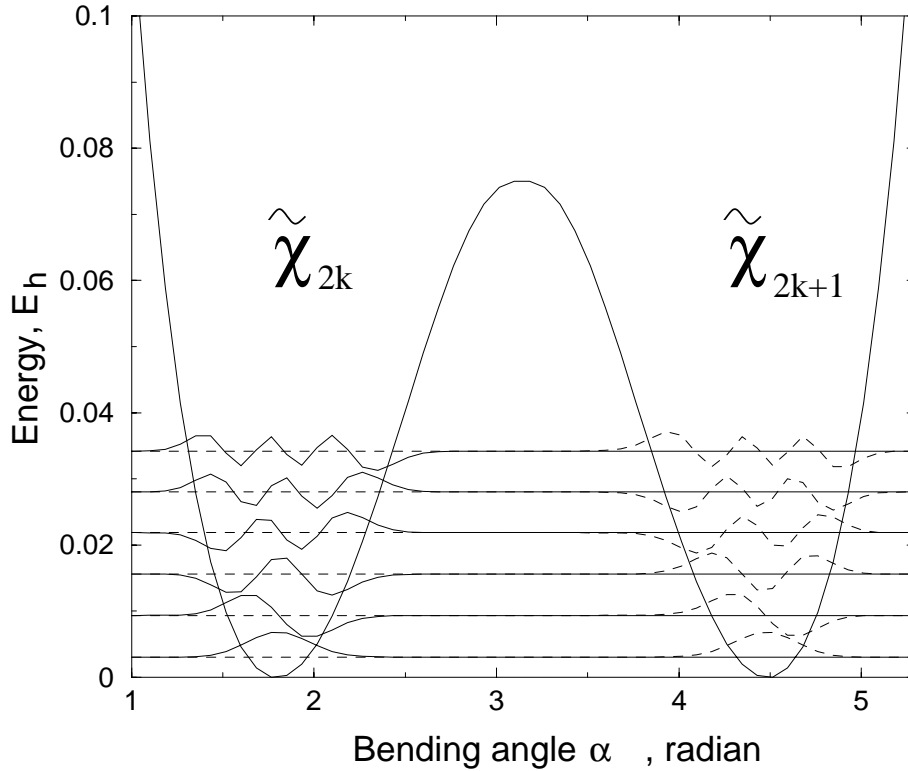


Figure 4.3: The localized linear combinations of the selected few degenerate low-lying zeroth-order bending states of HONO₂

eigenfunctions $|\chi_k^0\rangle$ form doublets of nearly degenerate states. For the purpose of analysis, the bending zeroth-order eigenfunctions shall be redefined as follows:

$$|\tilde{\chi}_{2k}^0\rangle = \frac{1}{\sqrt{2}}(|\chi_{2k+1}\rangle + |\chi_{2k}\rangle), \quad (4.23)$$

$$|\tilde{\chi}_{2k+1}^0\rangle = \frac{1}{\sqrt{2}}(|\chi_{2k+1}\rangle - |\chi_{2k}\rangle), \quad (4.24)$$

see reference [110]. The even-numbered states $|\tilde{\chi}_k^0\rangle$, $k = 0, 2, 4, \dots$ are then local-

ized in one well of the double-minimum potential, whereas the odd-numbered ones, $|\tilde{\chi}_k^0\rangle$, $k = 1, 3, 5, \dots$, are located in the other well, which is separated by the barrier of the 2.04 eV height (see Figure 4.3). Thus defined, the wave functions $|\tilde{\chi}_k^0\rangle$ describe two energetically equivalent conformers of the HONO₂ molecule [110].

We shall henceforth use the following notation

$$|n, m, k\rangle = |\psi_n^0\rangle|\phi_m^0\rangle|\tilde{\chi}_k^0\rangle \quad (4.25)$$

for the 3-D direct product zeroth-order states. The $|0, 0, 0\rangle$ zeroth-order state was propagated in imaginary time [74] to obtain the ground vibrational state Φ_0 , an initial state for quantum molecular dynamics simulations.

The HONO₂ molecule is considered lying in the (x, y) plane and preoriented in such a way that the ON single bond is parallel to the x axis. Such an orientation can be achieved, for example, by subjecting the initial ensemble of molecules to an external direct current (DC) electric field [120]. The electric field of the laser is assumed to be linearly polarized and aligned in the (x, y) plane with an angle β to the x axis. The interaction of the molecule with the laser field is treated semiclassically within the electric dipole approximation by the interaction Hamiltonian

$$\hat{H}_{\text{int}}(r_1, r_2, \alpha, t) = -\mathcal{E}(t)[d_x(r_1, r_2, \alpha) \cos \beta + d_y(r_1, r_2, \alpha) \sin \beta], \quad (4.26)$$

where $d_x(r_1, r_2, \alpha)$ and $d_y(r_1, r_2, \alpha)$ are the components of the dipole function along the x and y axes, defined *ab initio* together with the potential energy surface $V(r_1, r_2, \alpha)$ [110], and $\mathcal{E}(t)$ is the electric field strength of the IR laser, defined as a single pulse of the type

$$\mathcal{E}(t) = \mathcal{E}_0 S(t) \cos(\omega_0 t), \quad (4.27)$$

where \mathcal{E}_0 is the (peak) amplitude of the pulse, ω_0 is the carrier frequency, and $S(t)$ is the shape function of the laser pulse.

4.1.3 Equation of motion and technique

The 3-D quantum dynamics of the molecule in the classical laser field $\mathcal{E}(t)$ is described by the time-dependent Schrödinger equation

$$i\hbar \frac{\partial}{\partial t} \Phi(r_1, r_2, \alpha, t) = [\hat{H}_{\text{mol}}(r_1, r_2, \alpha) + \hat{H}_{\text{int}}(r_1, r_2, \alpha, t)] \Phi(r_1, r_2, \alpha, t), \quad (4.28)$$

where the molecular Hamiltonian \hat{H}_{mol} and the interaction Hamiltonian \hat{H}_{int} are defined by equations (4.1), (4.15) and (4.26) respectively.

The wave function and operators of the equation (4.28) have been represented on a $256 \times 32 \times 64$ -point spatial grid for r_1, r_2 and α coordinates respectively. The time-dependent Schrödinger equation (4.28) was solved by split-operator method [54] with several modifications to enable the evaluation of mixed kinetic energy terms [58]. The time step of propagation ranged from 0.3 to 1.5 atomic time units.

At large values of the dissociative coordinate r_1 we use an imaginary optical potential of the kind

$$U_1^{\text{opt}} = -iU_0 \exp\{(3/2)[1 - (r_1^{\text{max}} - r_1^{\text{opt}})^2 / (r_1 - r_1^{\text{opt}})^2]\}, \quad (4.29)$$

if $r_1 \geq r_1^{\text{opt}}$, and $U_1^{\text{opt}}(r_1) = 0$ otherwise [121]. A similar absorbing boundary condition was also provided for large values of r_2 . In practice, however, the wave packets never approached the outer end of the r_2 coordinate.

The time-dependent populations of the zeroth-order vibrational states of the molecule are defined by projection of the time-dependent wave function $\Psi(t)$ on the respective zeroth-order states $|n, m, k\rangle$ as follows:

$$P_{(n,m,k)}(t) = \int_{r_1^{\text{min}}}^{r_1^{\text{opt}}} \int_{r_2^{\text{opt}}}^{r_2^{\text{max}}} \int_{\alpha^{\text{min}}}^{\alpha^{\text{max}}} |\langle k, m, n | \Phi(t) \rangle|^2 dr_1 dr_2 d\alpha, \quad (4.30)$$

As a measure of the degree of excitation in different vibrational modes, the use is made of overall excitation probabilities in certain degrees of freedom, defined as

$$P_{\text{ON}}(t) = \sum_{n>0} P_{(n,0,0)}(t) \quad (4.31)$$

for the ON bond, and

$$P_b(t) = \mathcal{N}(t) - \int_{r_1^{\min}}^{r_1^{\text{opt}}} \int_{r_2^{\min}}^{r_2^{\text{opt}}} \int_{\alpha^{\min}}^{\alpha^{\max}} (|\langle \tilde{\chi}_0^0(\alpha) | \Phi(t) \rangle|^2 + |\langle \tilde{\chi}_1^0(\alpha) | \Phi(t) \rangle|^2) dr_1 dr_2 d\alpha, \quad (4.32)$$

for the bending degree of freedom.¹ Here $\mathcal{N}(t)$ is the norm of the wave function remaining on the grid (excluding the absorbing boundary regions), given by the expression

$$\mathcal{N}(t) = \int_{r_1^{\min}}^{r_1^{\text{opt}}} \int_{r_2^{\min}}^{r_2^{\text{opt}}} \int_{\alpha^{\min}}^{\alpha^{\max}} |\Phi(r_1, r_2, \alpha, t)|^2 dr_1 dr_2 d\alpha. \quad (4.33)$$

Two zeroth-order states $\tilde{\chi}_0^0$ and $\tilde{\chi}_1^0$ appear in the equation (4.32) because of the degenerate character of bending vibrational eigenfunctions.

4.2 Evolution and preparation of zeroth-order vibrational states

In this section the Hamilton operator derived in Section 4.1.1, together with the techniques described above, shall be applied to the problem of preparation and evolution of zeroth-order OH states of HONO₂. The zeroth-order states play an important role in mode-selective chemistry and molecular spectroscopy [11, 122–125], for several reasons. Firstly, by definition, they represent molecular states, in which the excitation is limited only to certain desired vibrational modes, which makes these states useful as an intermediate steps in photochemical reactions, for example. Secondly, the zeroth-order states, in contrast to molecular eigenstates, are not stationary, and can couple with other modes, which manifests itself in characteristic oscillations, or quantum beats [10, 11, 126]. The analysis of these oscillations yields

¹The formula (4.32) has its origins in the projection method as defined by the equation (2.20). The total 3-D wave function is projected on the bending degree of freedom, where the overlap with the ground zeroth-order state is calculated. The higher the degree of bending excitation, the smaller the overlap. For the low-lying zeroth-order states considered here the norm remaining on the grid was always equal to one.

information on the energies of states, to which the zero-order state is coupled, and also the strengths of these couplings. The number of vibrational states which are efficiently coupled can in many cases be quite small, which corresponds to the case of restricted IVR [127].

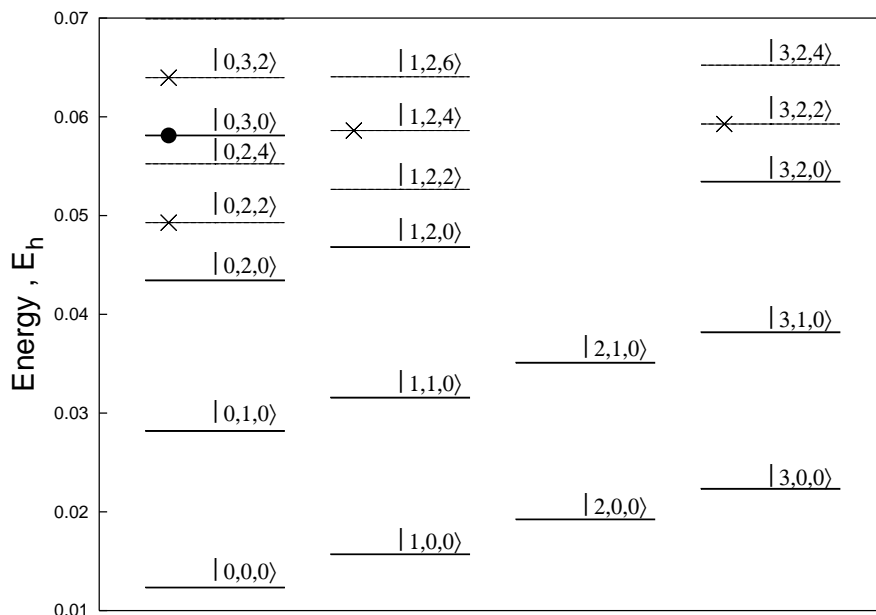


Figure 4.4: Low lying vibrational zeroth-order states of the HONO₂ molecule. The circle denotes the initial $|0, 3, 0\rangle$ zeroth-order state, and cross-markers denote the states efficiently coupled to the initial one.

The restricted IVR in HONO₂ molecule shall be illustrated on the example of the $|0, 3, 0\rangle$ zeroth-order state, which has three vibrational quanta in the local OH bond, and the other vibrational degrees of freedom are not excited. The energy of this state lies well below the dissociation threshold, and the density of states in this region is small, which means that rather few states may participate in restricted IVR. The energy level diagram in the vicinity of the $|0, 3, 0\rangle$ state is presented in figure 4.4. We note, that there are only a few states in the vicinity of the $|0, 3, 0\rangle$ state, and the closest lying $|1, 2, 4\rangle$ and $|3, 2, 2\rangle$ zeroth-order states should be quite strongly coupled to the chosen $|0, 3, 0\rangle$ state. Which other states also play an important role in the restricted IVR, shall be clarified below.

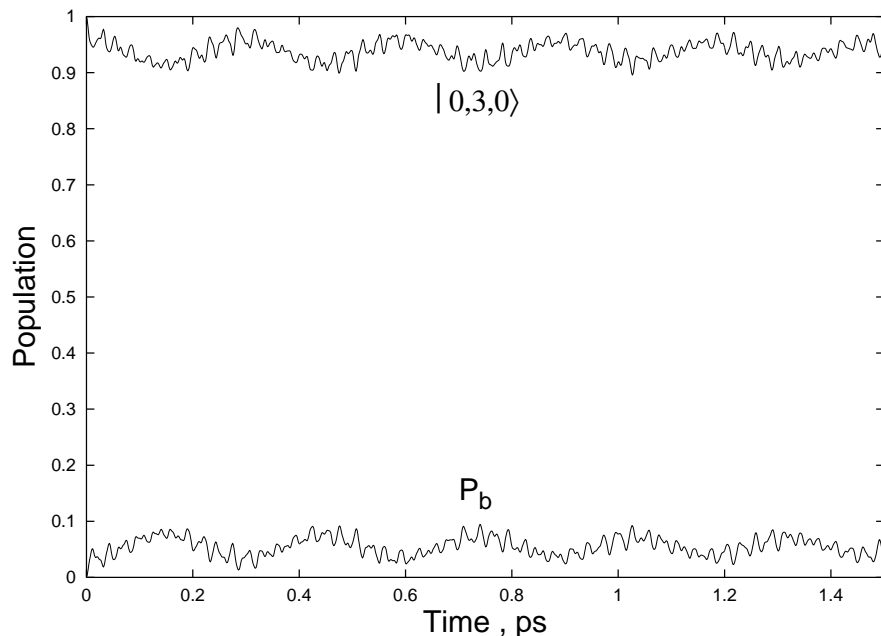


Figure 4.5: Free evolution of the $|0, 3, 0\rangle$ zeroth-order state, compared to the time-dependent probability of the excitation of the bending degree of freedom $P_b(t)$.

First, the free evolution of the $|0, 3, 0\rangle$ state was studied, assuming that it was already prepared selectively. The dynamics of this process is presented in Figure 4.5. The bottom curve in Figure 4.5, is the overall probability of the excitation of the bending degree of freedom, defined by equation (4.32). We see the characteristic quantum beat pattern, which consists of several harmonics, suggesting that several vibrational zeroth-order states are involved in restricted IVR. Also, the $P_b(t)$ curve is out of phase with the $P_{(0,3,0)}$, which indicates, that the vibrations in the bond lengths are primarily coupled via the bending mode, a manifestation of the heavy-atom blocking effect of the central oxygen atom. The relatively small amplitude of the oscillations suggests a comparatively weak coupling between the bending and two stretching degrees of freedom at the energies close to that of the $|0, 3, 0\rangle$ state.

Let us now attempt to establish, which zeroth-order states dominate the restricted IVR. This is achieved by free propagation of several selected zeroth-order states, with energies close to that of the state $|0, 3, 0\rangle$. By this means, four states were selected, marked on the Figure 4.4 by cross-markers. The time evolution of these

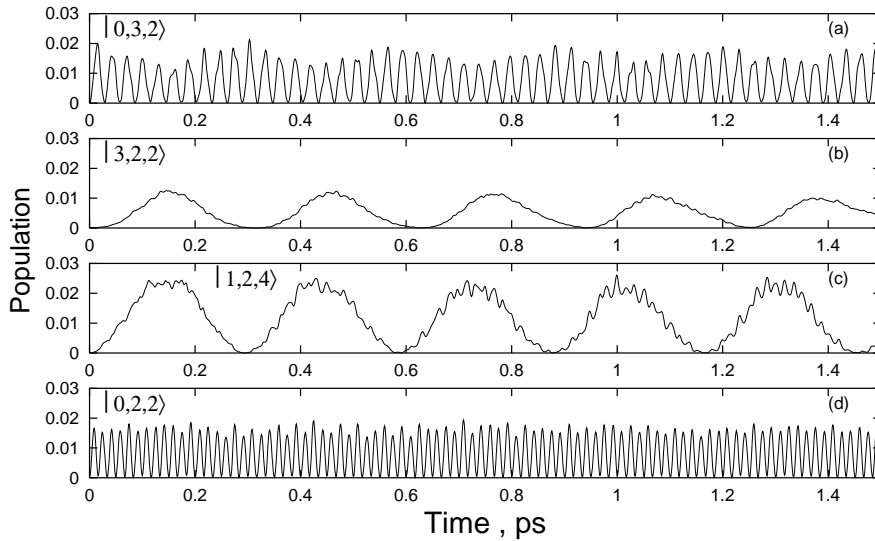


Figure 4.6: Population dynamics of selected low-lying zero-order states of HONO₂ molecule. The states are arranged in descending order by energy.

states is presented in Figure 4.6. Previous studies of restricted IVR [11, 125] point at the following characteristics of quantum beats: the frequency of the oscillations is determined by the energy difference between the two coupled zero-order states, and the amplitude is determined by the strength of the coupling [11, 125]. The Figure 4.6 clearly illustrates these tendencies: the two states closest to $|0, 3, 0\rangle$, i.e. $|1, 2, 4\rangle$ (Figure 4.6b) and $|3, 2, 2\rangle$ (Figure 4.6c) provide the dominant low-frequency contribution to the total bending excitation probability, and the two other states, $|0, 3, 2\rangle$ (Figure 4.6a) and $|0, 2, 2\rangle$ (Figure 4.6d) are responsible for the high-frequency low-amplitude modulation. To prove that the four zeroth-order states marked on Figure 4.4 are indeed the ones most efficiently coupled to the $|0, 3, 0\rangle$ state, we compare their combined contribution

$$P_{\text{sum}}(t) = P_{(0,3,2)}(t) + P_{(3,2,2)}(t) + P_{(1,2,4)}(t) + P_{(0,2,2)}(t) \quad (4.34)$$

with the total bending excitation probability (Figure 4.7). As we can see, taking into account the contributions from the four states most efficiently coupled to $|0, 3, 0\rangle$ reproduces the features of the out-of-phase oscillations in the bending mode quite adequately. The difference between $P_{\text{sum}}(t)$ and $P_b(t)$ diminishes, when more zeroth-

order states are taken into account.

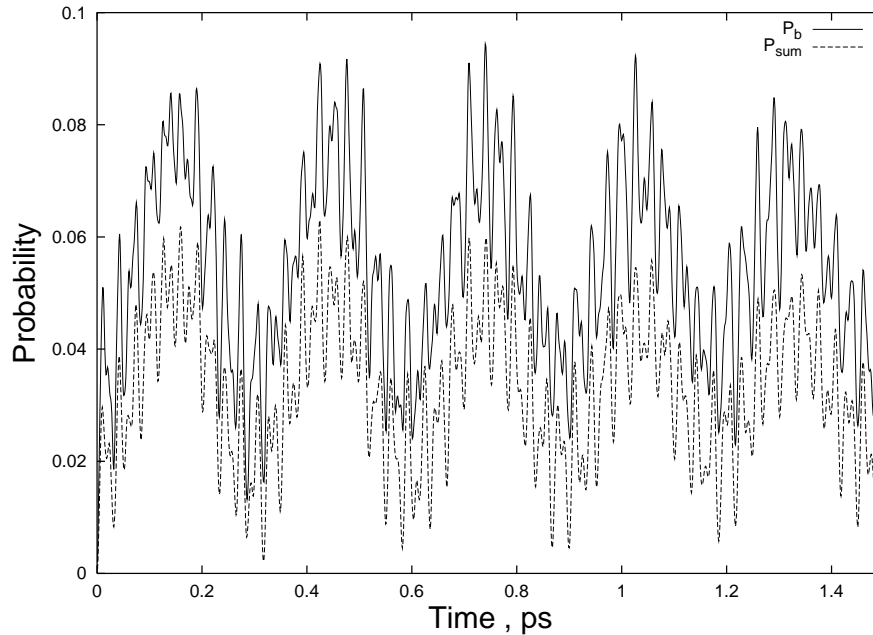


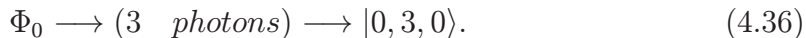
Figure 4.7: Comparison of the total time-dependent bending excitation probability $P_b(t)$ (solid line) with the combined contribution from four selected zeroth-order states $P_{\text{sum}}(t)$ (dashed line), see Eqn. (4.34).

So far the free evolution of the $|0, 3, 0\rangle$ zeroth-order OH state was considered. It is also possible to prepare this state selectively, using a short sine-squared shaped laser pulse. The task of selective preparation of zeroth-order state is more complex than that of eigenstate preparation, because in order to prepare a zeroth-order state one has to utilize short intense pulses to compete against IVR, at the expense of spectral selectivity. Nevertheless, such preparation is feasible, which was demonstrated previously both experimentally [11, 127–131] and theoretically [11, 125, 127]. The use of a laser pulse with the sine-squared envelope shall be made, when the shape function $S(t)$ in the equation (4.27) is:

$$S(t, \tau_p) = \sin^2 \left(\frac{\pi t}{\tau_p} \right), \quad (4.35)$$

where τ_p is the duration of the pulse. The electric field axis of the linearly polarized laser field was aligned along the OH bond of the HONO₂ molecule.

The preparation of the $|0, 3, 0\rangle$ zeroth-order state is demonstrated in Figure 4.8. The excitation proceeds along the following pathway:



The sine-squared shaped laser pulse of the duration $\tau_p = 0.3$ ps, frequency $\omega_0 = 3351.60 \text{ cm}^{-1}$ and amplitude $\mathcal{E}_0 = 110.56 \text{ MV/cm}$ was used (see figure 4.8c). The optimal laser fields were designed by G.K. Paramonov [116, 117]. Shown on the Figure 4.8a are the population of the target zeroth-order state $P_{(0,3,0)}$, the population of the vibrational ground state of the HONO₂ molecule P_0 , and the total probability of the excitation of the bending degree of freedom.

Analogously to the case of the free evolution, the $P_{(0,3,0)}(t)$ and $P_b(t)$ curves display the in- and out-phase oscillatory behaviour. The vibrational ground state retains about 15% of the population, which does not influence the IVR, since the population is confined in an eigenstate. The character of the quantum beats is only slightly different from the case of free evolution in a sense, that the high-frequency modulation of the oscillating populations is much less pronounced, when the molecule is prepared with a laser. The origin of the difference lies in the process of preparation of the target zeroth-order state with the laser light, during which the intramolecular coherency is induced [11, 125]. The contributions from the four zeroth-order states involved most efficiently in restricted IVR are presented in figure 4.8b. One can observe, that the amplitudes of the high-frequency components $|0, 3, 2\rangle$ and $|0, 2, 2\rangle$ are indeed much less than in the case of free evolution, indicating their efficient averaging by the laser field, which has frequency close to that of the population oscillations.

4.3 Selective breaking of the ON bond

Another important aspect of the model discussed in this work is its suitability for problems involving large amplitude motions of a molecule, including those of the laser-induced dissociation. In this section we shall demonstrate this by considering

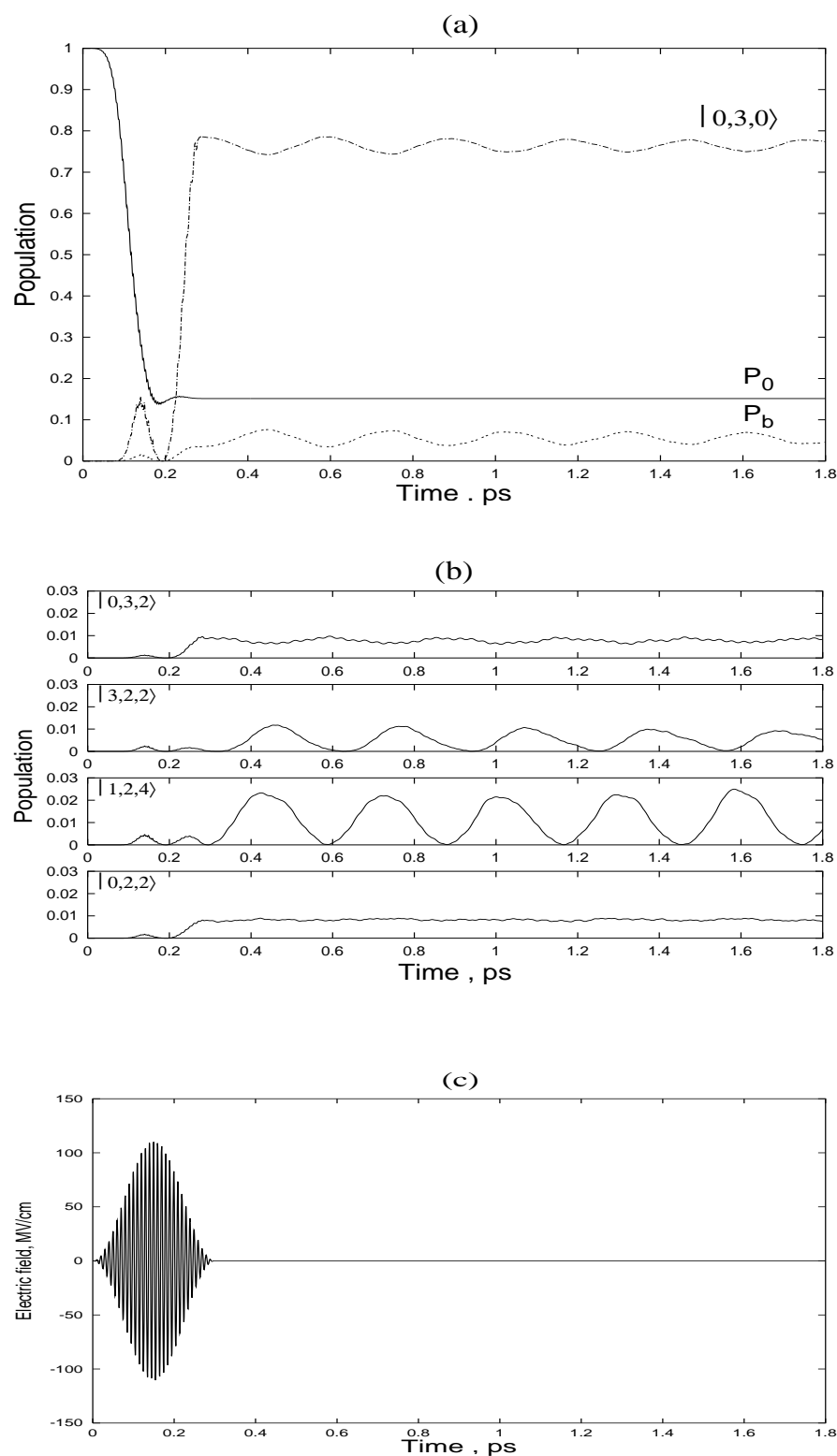


Figure 4.8: Selective preparation of the $|0, 3, 0\rangle$ zeroth-order state. (a) Population dynamics. P_0 and P_b denote the population of the ground vibrational state and the total bending excitation probability, respectively; (b) Population dynamics of selected zeroth-order OH states most efficiently involved in IVR; (c) Optimal laser field: $\tau_p = 0.3$ ps, $\omega_0 = 3351.60$ cm^{-1} , $\mathcal{E}_0 = 110.56$ MV/cm.

the process of ON single bond breaking. Instead of a sine-squared type pulse, use shall be made of a laser field with the following shape function:

$$S(t, \tau_s, \tau_{pl}, \tau_p) = \begin{cases} \sin^2(\pi t/2t_s) & \text{if } 0 \leq t \leq t_s \\ 1 & \text{if } t_s \leq t \leq t_s + t_{pl} \\ \sin^2(\pi(t - t_{pl})/2t_s) & \text{if } t_s + t_{pl} \leq t \leq t_p \end{cases} \quad (4.37)$$

Such plateau-type pulses with sine-squared switch-on and switch-off proved to be more suitable for efficient control of molecular dissociation than purely sine-squared type pulses of the same duration [110,117]. The shape parameters of the pulse (4.37) have been optimized by Dr. G.K. Paramonov together with the amplitude and the carrier frequency to maximize the dissociation yield. The electric field axis of the linearly polarized laser field has been aligned along the ON single bond.

As a measure of the dissociation yield, we take the integrated outgoing flux, which is monitored at the position of the beginning of the absorbing boundary in NO bond length:

$$D(t) = \frac{\hbar}{\mu_1} \int_0^t dt' \int_{r_2^{\min}}^{r_2^{\max}} dr_2 \int_{\alpha^{\min}}^{\alpha^{\max}} d\alpha \operatorname{Im} \left(\Phi^*(r_1, r_2, \alpha, t') \frac{\partial \Phi(r_1, r_2, \alpha, t')}{\partial r_1} \right) \Big|_{r_1=r_1^{\text{opt}}} \quad (4.38)$$

At any given time the consistency check

$$\mathcal{N}(t) + D(t) = 1, \quad (4.39)$$

was fulfilled with better than 1% accuracy.

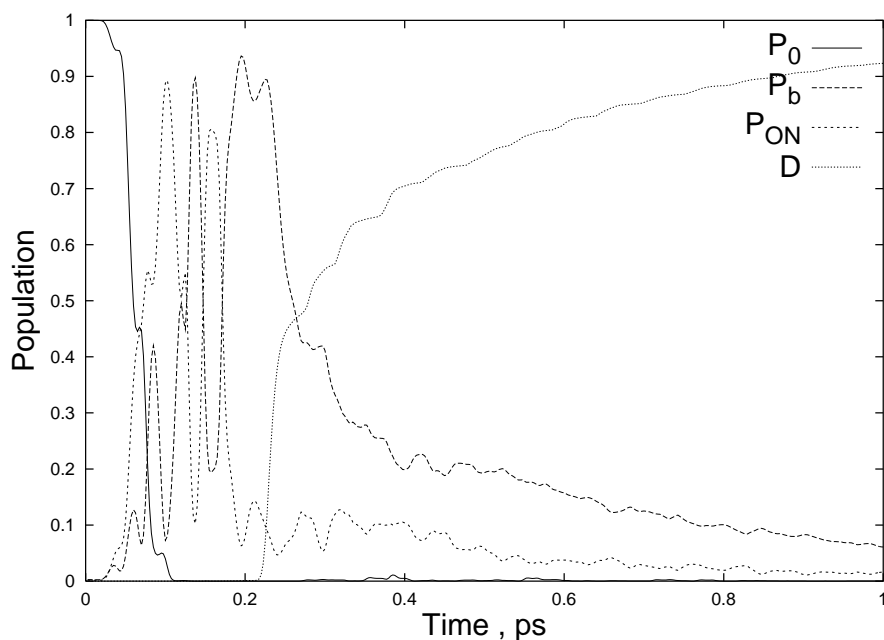
The results for the selective breaking of ON bond are presented in figure 4.9a. The laser excitation has a resonant character, with the pathway given by

$$\Phi_0 \longrightarrow (27 \text{ photons}) \longrightarrow |30, 0, 0\rangle \longrightarrow \text{continuum}. \quad (4.40)$$

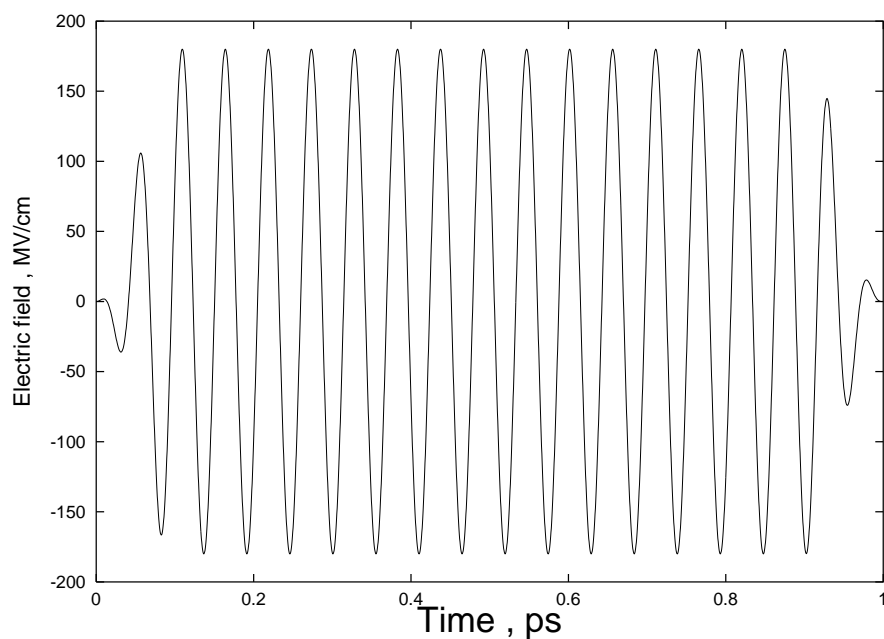
The duration of the pulse was $\tau_p = 1$ ps, which includes the sine-squared type switch-on and switch-off of the duration $\tau_s = 0.1$ ps and 0.8 ps plateau. The laser carrier frequency was $\omega_0 = 609.92 \text{ cm}^{-1}$, and the peak amplitude $\mathcal{E}_0 = 179.98$

MV/cm. As we can see, a single plateau-like laser pulse leads to highly efficient (93% probability) dissociation. The laser pulse is shown in Figure 4.9b.

It is worth noting, that the behaviour of the excitation probabilities in the ON and bending modes indicate an efficient interchange of energy, which manifests itself in strongly modulated, almost out-of-phase oscillations of the respective probabilities during the initial stages of laser excitation ($0.05 \text{ ps} < t < 0.2 \text{ ps}$). After the first 0.2 ps, the excitation is transferred mainly to the bending degree of freedom (curve ' P_b '), and shortly afterwards the molecule starts to dissociate. The fact that the bending mode of vibration plays a very important role in the energy redistribution highlights the advantages of the model presented here, since it allows accurate treatment of bending vibrations, including the large amplitude ones. The OH bond stretching degree of freedom remains unexcited, and plays a negligible role in the process of selective ON bond breaking.



(a)



(b)

Figure 4.9: Breaking of the ON single bond. (a) Population dynamics. P_0 is the population of the vibrational ground state, P_{ON} and P_b are the excitation probabilities of ON single bond and the bending mode respectively, D is the dissociation yield; (b) Optimal laser field: $\tau_p = 1$ ps, $\tau_s = 0.1$ ps, $\tau_{pl} = 0.8$ ps, $\omega_0 = 609.92$ cm⁻¹, $\mathcal{E}_0 = 179.98$ MV/cm.